Temperature-Dependent Microstructural Evolution of Al-Rich Medium-Mn Steel During Intercritical Annealing

Skowronek, Adam; Grajcar, Adam; Kozłowska, Aleksandra; Janik, Aleksandra; Morawiec, Mateusz; Petrov, Roumen H.

DOI
10.1007/s11661-022-06721-2

Publication date
2022

Document Version
Final published version

Published in
Metallurgical and Materials Transactions A: Physical Metallurgy and Materials Science

Citation (APA)
Skowronek, A., Grajcar, A., Kozłowska, A., Janik, A., Morawiec, M., & Petrov, R. H. (2022). Temperature-Dependent Microstructural Evolution of Al-Rich Medium-Mn Steel During Intercritical Annealing. *Metallurgical and Materials Transactions A: Physical Metallurgy and Materials Science*, *53*(8), 3012-3021. https://doi.org/10.1007/s11661-022-06721-2

ORIGINAL RESEARCH ARTICLE

Temperature-Dependent Microstructural Evolution of Al-Rich Medium-Mn Steel During Intercritical Annealing

ADAM SKOWRONEK, ADAM GRAJCAR, ALEKSANDRA KOZŁOWSKA, ALEKSANDRA JANIK, MATEUSZ MORAWIEC, and ROUMEN H. PETROV

Medium-Mn automotive sheet steels require optimized heat-treatment processes to obtain benefits caused by strain-induced martensitic transformation of retained austenite (RA) during sheet metal forming or crash events. The intercritical annealing (IA) approach at different temperatures in a range of 640 °C to 800 °C is proposed in the study for a 5Mn hot-rolled medium-Mn sheet steel. The experiments were performed in terms of dilatometry. The analysis of the cooling curves allowed development of a new method for calculating the high-temperature phase equilibrium. The calculations were validated by modeling with JMatPro and experimentally verified by X-ray diffraction (XRD). The microstructure evolution was characterized using light optical microscopy and scanning electron microscopy (SEM), including electron backscatter diffraction (EBSD). The quantitative determination of the fraction, morphology, chemical composition, and stability of the RA was done. Mechanical properties were determined by hardness measurements. The research showed a substantial influence of the IA temperature on the RA fraction and chemical stability and properties of medium-Mn Al-alloyed steel. At temperatures of 680 °C and 700 °C, the largest fraction of over 35 pct of stable RA was obtained, which does not transform to martensite during cooling.

https://doi.org/10.1007/s11661-022-06721-2

I. INTRODUCTION

THE heat treatments of novel medium-Mn automotive sheet steels are quenching and partitioning (QP),[1] thermomechanical processing (TMP),[2,3] and intercritical annealing (IA).[4] IA allows the largest amounts of retained austenite (RA) to be obtained in the microstructure[5] by significant enrichment of this phase with carbon from intercritical ferrite.[6] For significantly long times, manganese partitioning[7] from the intercritical ferrite can also take place, resulting in additional reduction of the martensite start (M_s) temperature below room temperature (RT). The thermally stable austenite, which transforms to martensite during deformation (forming/road collision), is crucial for the mechanical and technological properties of the medium-Mn sheet steels.

The medium-Mn steel sheets produced by this method can be used for elements of controlled crumple zones, which must ensure high energy absorption, both through their properties and through part design approaches.[8] A very good combination of strength and ductility allows the production of geometrically complicated body parts.[9] The strain-induced martensitic transformation due to the mechanically metastable RA leads to strong strengthening of the material during pressing, bending, *etc*. Therefore, the final parts may be characterized by advanced geometry, guaranteeing stiffness and strength, enhanced by the increased strength of the material itself. The part of the RA characterized by high stability remains in the material during forming operations, while the one with low stability transforms to martensite. The former is

ADAM SKOWRONEK, ADAM GRAJCAR, and ALEKSANDRA KOZŁOWSKA are with the Department of Engineering Materials and Biomaterials, Faculty of Mechanical Engineering, Silesian University of Technology, Konarskiego 18a St., 44-100, Gliwice, Poland. Contact e-mail: adam.grajcar@polsl.pl ALEKSANDRA JANIK is with the Łukasiewicz Research Network-Institute for Ferrous Metallurgy, 12-14 K. Miarki Street, 44-100 Gliwice, Poland. MATEUSZ MORAWIEC is with the Materials Research Laboratory, Faculty of Mechanical Engineering, Silesian University of Technology, Konarskiego 18a St., 44-100 Gliwice, Poland. ROUMEN H. PETROV is with the Department of Electromechanical, Systems and Metal Engineering, Research Group Materials Science and Technology, Ghent University, Tech Lane Ghent Science Park, Campus A, Zwijnaarde, Technologiepark 46, 9052 Ghent, Belgium and also with the Department of Materials Science and Engineering, Delft University of Technology, 3mE-TUDelft, Building 34, Mekelweg 2, 2628 CD, Delft, The Netherlands.
Manuscript submitted January 21, 2022; accepted May 8, 2022.
Article published online June 13, 2022

expected to absorb a part of the energy during possible crush events, generating high deformations.[10]

Unlike QP and TMP processes, which require more technological steps, such as isothermal holdings during cooling or reheating, IA is a very simple final treatment process that usually consists of one annealing step followed by quenching. What is more, it may be applied to both hot- and cold-rolled steels. Due to the increased content of Mn in these steels, and thus very high hardenability,[11] even significant differences in the cooling rate usually do not cause technological problems (such as the formation of unwanted phases in the material). This is very important for industrial applications, the conditions of which may differ from laboratory ones.[12] The parameters of IA (such as heating and cooling rate,[13] IA temperature effect,[14] IA soaking time effect,[13] and initial microstructure[15]) have a critical impact on the obtained microstructure of steel,[16] on the chemical composition of individual phases,[17] and, thus, on the mechanical properties of the final product. The paramount parameters of IA for this specific group of steels are temperature and time of the process. Both of these are used to control the chemical element redistribution between the ferrite and intercritical austenite, as well as the fraction of RA.[18] When the temperature is increased, the γ (intercritical austenite)/α (ferrite) ratio increases according to the phase equilibrium system. Using a too low temperature will provide a low fraction of very stable RA (strongly enriched with carbon and, in this case, with manganese), which is very difficult to transform into martensite. Thus, the target properties of the material will be lowered. Increasing the temperature too much will cause the formation of a large fraction of intercritical austenite with the low C and Mn contents, which is expected to have low thermal and mechanical stability. Such low-stable austenite is prone to partial or complete transformation to martensite during cooling.[13] For this reason, it is very important to define the technological window for a given steel, which will ensure both the appropriate fraction and stabilization of RA.

The Si or Al additions in medium manganese steels are often used to prevent the formation of carbides. These elements limit the nucleation and inhibit the growth of carbides, so that both carbon and manganese can enrich austenite.[13] However, Si has some disadvantages compared to Al. The main one is the difficulty in hot-dip galvanizing of Si-based alloys.[19] Moreover, aluminum increases the A_{c1} and A_{c3} temperatures, which accelerates diffusion and enables faster achievement of the equilibrium state.[13] In addition, extending the intercritical range increases the temperature range of the mentioned technological window,[20] which results in a lower sensitivity of the process to possible deviations of process parameters.

Despite numerous research methods, it is still difficult to precisely determine the proportion of phases in the intercritical region, which is important during the introduction of a new steel grade to production and could, among other things, speed up the optimization of new steel grade development. One of the methods is X-ray diffraction (XRD) performed at elevated temperatures, which monitors the current state of the sample (*in situ*).[21,22] Another method includes thermodynamic calculations, which, however, have to be further validated experimentally. The dilatometric method is a highly effective and accurate way of providing information on linear thermal expansion of tested samples. It is correlated with various processes and phase transformations taking place in material[23] and is commonly used for heat-treatment simulations. However, it should be noted that thermal expansion is also characteristic of a given phase, which can be used (after determining the boundary conditions for the investigated material) to determine its amount in the structure.

The first aim of the current study is to characterize the microstructure of hot-rolled Al-rich medium-Mn steel after different heat-treatment processes. These processes differ in the IA temperature, which influences the RA fraction, impacts the chemical composition of the intercritical austenite, and determines its morphology and stability. The second goal is to confirm a novel method concerning the correlation of the thermal expansion of cooled samples in different phase states with the percentage of these phases in the microstructure. The research was supplemented with thermodynamic calculations and XRD measurements validating the results theoretically and experimentally.

II. EXPERIMENTAL PROCEDURES

A. *Material*

The chemical composition of the analyzed medium-Mn steel is presented in Table I. The content of individual chemical elements was designed to obtain the best alloy properties, considering its automotive sheet application. The relatively low carbon content prevents a marked reduction in weldability.[24] The Mn content of 4.7 wt pct was added to increase the RA stability while not causing a large increase in the price of the material.[25] The typical Mn additions in this kind of steel are in the 5 to 12 pct Mn range.[13] The Si and Al were added to prevent the carbide precipitation, but the low Si content was applied due to its negative influence on hot-dip galvanizing.[19] The tested steel was produced using a Balzers vacuum furnace (mold with the following dimensions: bottom—122-mm o.d., top—145-mm o.d., and height—200 mm). Next, 25-kg ingot was forged in a temperature range from 1200 °C to 900 °C (155 mm × 23 mm). Finally, material was hot rolled in a temperature range from 1100 °C to 750 °C to a thickness of 4.5 mm, imposing ~80 pct reduction, and air cooled, which ensures formation of a fully martensitic structure due to the high hardenability caused by Mn addition. The martensitic microstructure is desirable due to the austenite reverse transformation (ART) process during IA.[26] Dilatometry samples with dimensions 4 × 10-mm o.d. were machined from the hot-rolled material with a long axis parallel to the plate rolling direction.

Table I. Chemical Composition of the Investigated Steel

Chemical Element (Wt Pct)							
C	Mn	Al	Si	Mo	S	P	Fe balance
0.16	4.7	1.6	0.20	0.20	0.005	0.008	93.12

Chemical composition was measured by optical emission spectroscopy after hot rolling.

B. *Heat Treatment*

The heat treatment was performed by the dilatometric method using a Bähr high-resolution DIL805A/D dilatometer. In the first experiment, a sample was heated to 1300 °C at 3 °C/s to determine the A_{c1} and A_{c3} temperatures. Next, based on the results, the heat-treatment cycles consisted of heating the samples at 3 °C/s, followed by an IA for 60 minutes at 640 °C/660 °C/680 °C/700 °C/720 °C/760 °C/800 °C/1100 °C. An annealing time of 1 hour was chosen to enable the redistribution of manganese, the diffusion of which is slow.[27] The last step of the process was rapid cooling of the samples (− 60 °C/s) to RT. The temperature was controlled by an S-type thermocouple, welded to the central part of each sample. The test was performed in vacuum, while helium was used for cooling the samples.

C. *Characterization of Phase Transformation and High-Temperature Equilibrium*

Theoretical calculations of the phase ortho-equilibrium at different IA temperatures were performed using JMatPro software with the implemented database v11.2; General Steels Module.[28] The simulation aim was to determine the theoretical relation of γ/α phases and their enrichment with stabilizing elements (C, Mn), which control the M_s temperature.

The dilatometric data were analyzed according to ASTM A1033-04.[29] Their main goal was to register the kinetics of phase transformations during the process and to calculate the linear expansion coefficient. The transformation start temperature was determined based on the measurement offset from the parallel line by 0.2 pct.[30]

The differential linear expansion coefficient α_L was calculated according to[31]

$$\alpha_L = \frac{\mathrm{d}L}{L_0 \times \mathrm{d}T}, 10^{-5} \times K^{-1} \qquad [1]$$

where α_L is the coefficient of linear thermal expansion, L_0 is the initial length of the sample, $\mathrm{d}L$ is the change in length of the sample, and $\mathrm{d}T$ is the change in the temperature.

To calculate the phase ratio during annealing, the following methodology was implemented. First, the differential linear expansion coefficient was calculated for each sample. Samples annealed at 640 °C and 1100 °C were considered as boundary conditions, as composed of 0 and 100 pct of austenite, respectively, based on the dilatometry curves. Only linear sections of the records were used for the calculations, ranging from 300 °C to 550 °C for each curve (the beginning, during which the cooling rate stabilizes, and the end, during which the martensitic transformation takes place in some samples, were not taken into consideration). Based on the range of the thermal linear expansion coefficient ($\alpha_{L\_100\ \mathrm{pct}} - \alpha_{L\_0\ \mathrm{pct}}$), the fraction of intercritical austenite (γ) was calculated for each of the samples, using

$$\gamma = \frac{100 \times (\alpha_{L_x} - \alpha_{L_{0\mathrm{pct}}})}{(\alpha_{L_{100\mathrm{pct}}} - \alpha_{L_{0\mathrm{pct}}})},\ \mathrm{pct} \qquad [2]$$

D. *Microstructural Characterization*

Standard metallographic preparation of the samples was performed prior to the observation. The samples were cut perpendicularly to their length and then mechanically ground (using SiC paper up to 2000 grid), polished (3, 1-μm paste, and colloidal silica), and etched in nital for 4 seconds at RT. Next, the samples were characterized by light optical microscopy using a Zeiss AxioObserver and scanning electron microscopy (SEM) by means of a Zeiss SUPRA 25. The images were taken in the central part of the sample (in half the plate thickness). Samples, after polishing with colloidal silica (OPS) for 15 minutes, were subjected to XRD analysis with a Panalytical X'Pert Pro MPD diffractometer and electron backscatter diffraction (EBSD) analysis with OIM TSL data collection software v. 7.3 installed on an FEI Quanta FEG 450 scanning electron microscope with a field emission gun filament. A sample tilt of 70 deg, working distance of 15 mm, accelerating voltage of 20 kV, and probe current of ~2.5 nA were used in all scans. Each scan was performed on an area of 5 × 10 μm^2 with a step size of 0.03 μm in a hexagonal scan grid. The orientation data were postprocessed with OIM TSL data analysis software v. 7.31 after applying a one-step grain confidence index (CI) standardization clean-up procedure. The points with CI < 0.1 were removed from the measurement, as they were dubious, and the remaining points, which were more than 99.5 pct, were analyzed. For XRD, the cobalt anode (λK_α = 0.179 nm) and the PIXcel 3D-detector on the diffracted beam axis were used. The diffraction lines were recorded in the Bragg–Brentano geometry in the angular range of 45 to 105 deg (2θ), with a step of 0.026 deg and scan speed of 0.6 s/step. The analysis of the obtained diffraction patterns was carried out using High Score Plus software v. 3.0 containing a dedicated inorganic crystal structure database (PAN-ICSD). The RA fraction determination was performed using the Rietveld refinement method. Based on the changes of the lattice parameter, the carbon concentration in austenite was calculated as follows[32]:

$$\alpha_\gamma = 3.556 + 0.0453x_C + 0.00095x_{\mathrm{Mn}} + 0.0056x_{\mathrm{Al}} \qquad [3]$$

where α_γ is in Å and x_C, x_{Mn}, and x_{Al} are the concentration of elements in austenite (weight percent).

The remaining parameters were typical.[33,34] Energy-dispersive X-ray spectroscopy (EDS) was

implemented to measure changes in Mn and Al concentrations in RA with increasing IA temperature (at least 15 measurements of different grains in random areas for each sample). To ensure the highest possible reliability of the results, the largest grains of RA were used for the measurements. Based on the determined concentration of both carbon and manganese, the theoretical M_s temperature of RA was calculated using the equation proposed in Reference 35:

$$M_s = 539 - 423 \times \mathrm{C} - 30.4 \times \mathrm{Mn} \qquad [4]$$

where C and Mn are in weight percent.

The variations in mechanical properties of the samples were characterized by monitoring the variations of the hardness as a function of the thermal treatment parameters. Vickers hardness was measured at a load of 1 kgf using the microhardness tester FB-700. Ten measurements for each sample were taken. Maximum and minimum values were excluded. For the remaining eight measurements, the average value was calculated.

III. RESULTS AND DISCUSSION

A. *Heat Treatment and RA Characterization*

Figure 1 presents the dilatometric heating curve of the investigated material. Two processes take place during heating: tempering and austenitization. One can see that after reaching 495 °C, the precipitation of carbides from the initial martensitic microstructure starts (third stage of tempering of martensite), and it ends at about 570 °C, causing a lattice contraction and, thus, changes in sample length.[36,37] From this measurement, A_{c1} and A_{c3} temperatures are determined as 648 °C and 924 °C, respectively. The addition of 1.5 pct Al causes an increase of A_{c1} and A_{c3} temperatures in the steel in comparison to the steel with 5 pct Mn and without Al, as reported elsewhere.[38]

Figure 2 presents the JMatPro simulations for equilibrium conditions at different IA temperatures. It can be seen that the content of the austenite stabilizing alloying elements (C, Mn) in the austenite decreases when the IA temperature increases (Figure 2(b)). This is related to the increasing fraction of austenite (Figure 2(a)) to which these elements are redistributed. This observation is in good agreement with earlier data provided by Lee and Han.[13] The decreased C and Mn contents of the intercritical austenite affect the M_s temperature, which increases due to the decelerating stability of γ.[4] The increase of the carbon content, which is visible in the first part of the graph (> 665 °C), is due to the dissolution of carbides. The theoretical results indicate that the highest annealing temperature at which the M_s is below 0 °C is about 683 °C and predicts the acquisition of 33 wt pct RA with the C and Mn enrichment at the levels of 0.51 and 9.6 wt pct, respectively.

Figure 3 presents dilatometric heating curves for all samples. The curves are in line with each other. Medium manganese steels are prone to manganese microsegregation.[39] Usually, the microsegregation causes large microstructural differences even in a sample treated in the same process and, thus, disrupts the compliance of dilatometric curves. In this case, this problem does not occur, which is important in the further analysis of the results.

The kinetics of austenite formation during IA is presented in Figure 4. It can be seen that the change in the length of samples treated at different temperatures is significantly different. The sample treated at 640 °C shows a change in length of ~0.14 pct. As evidenced by the measured A_{c1} temperature at 640 °C, austenite

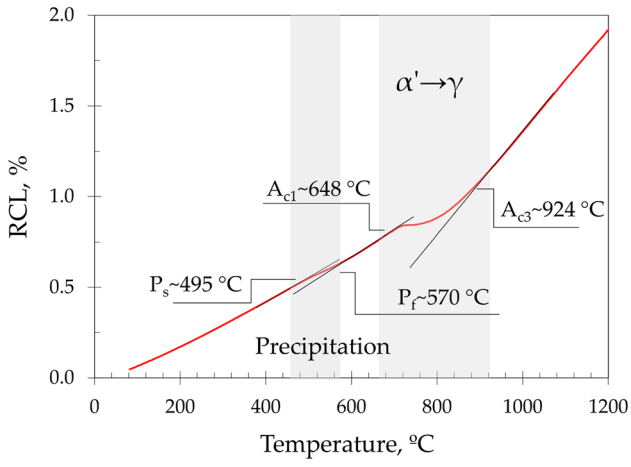

Fig 1—Dilatometric heating curve of investigated material; $P_{s,f}$—precipitation start/finish; RCL—relative change in length.

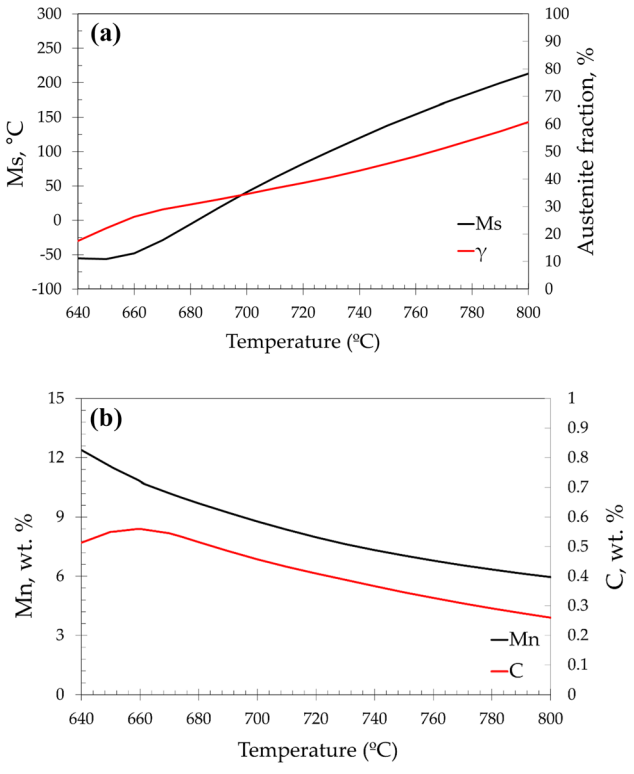

Fig. 2—Results of theoretical calculations of (*a*) the M_s and γ fraction and (*b*) Mn and C concentrations in the γ as a function of the annealing temperature.

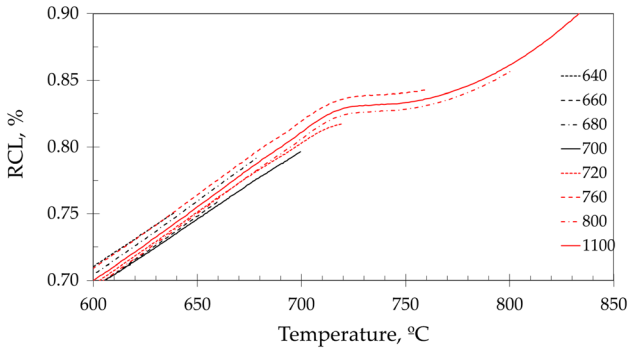

Fig. 3—Dilatometric heating curves of the samples annealed at different temperatures.

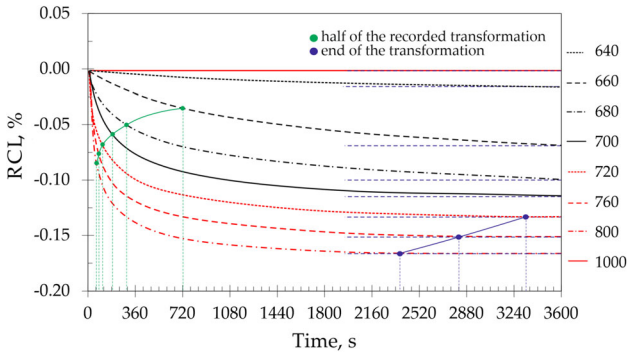

Fig. 4—Dilatometric curves of the samples annealed at different temperatures; green dots mark the time of 50 pct change in relative sample length, and violet dots mark the time of completion of changes in sample relative length (Color figure online).

should not be formed. The recorded change in sample length may be associated with the further tempering and carbide precipitation,[40,41] which were indicated by the heating curve. When the IA is increased, the transformation kinetics intensifies significantly. Because the applied temperatures are higher than A_{c1}, we can assume that the changes are caused by austenite formation. The curves were described by means of two characteristics: the half time of the transformation (green markings) and its completion (if there is any, violet markings). The sample annealed at 660 °C reaches half of the recorded transformation after ~12 minutes. It is visible that after 1 hour of annealing, the transformation is still not completed, as the curve does not reach plateau (maximum RCL is − 0.07 pct). The transformation is completed only in a sample treated at 720 °C (after 55.5 minutes), where the half transformation time is ~110 seconds. With a further increase of the annealing time, the transformation end temperature is reduced to ~39.5 minutes and the half transformation time to ~63 seconds in a sample IA800 (maximum RCL is − 0.165 pct). The sample treated at 1000 °C does not exhibit any changes in sample length during annealing, as the temperature is higher than A_{c3}.

Figure 5 presents the dilatometric cooling curves of the tested samples. The records related to cooling of samples annealed at temperatures from 640 °C to 700 °C do not show any transformations. The rapid increase in

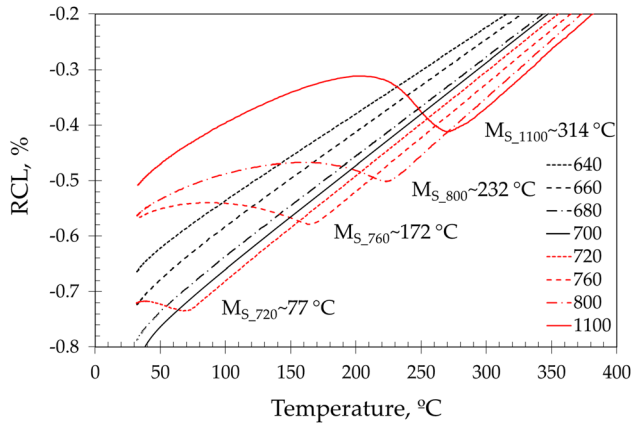

Fig. 5—Dilatometric cooling curves of the samples annealed at different temperatures.

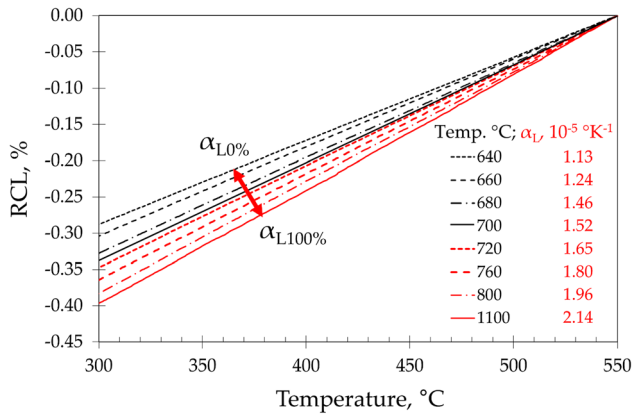

Fig. 6—Dilatometric results showing the slope of the curves at different annealing temperatures and corresponding calculated linear expansion coefficient.

the elongation related to the start of martensitic transformation appears in the curves for the samples annealed at temperatures higher than 700 °C. The M_s temperature and the rate of transformation increase with the increase of annealing temperature (Figure 5). This is related to an increased fraction of low-stable austenite, less enriched in austenite stabilizing elements. For all samples, the thermal linear expansion coefficient was calculated in the range of 550 °C to 300 °C to avoid regions where martensitic transformation and initial stabilization of the cooling rate occur (Figure 6). Samples annealed at the temperatures of 640 °C and 1100 °C were prepared as "boundary" samples referring to 100 pct of ferrite and 100 pct austenite, respectively, according to the dilatometric results. The coefficient of linear thermal expansion for 100 pct ferrite was 1.13×10^{-5} K^{-1} and for 100 pct austenite was 2.14×10^{-5} K^{-1}. These results are in agreement with the literature data, α_L, for austenite, 2.25×10^{-5} K^{-1},[31] 2.09×10^{-5} K^{-1},[42] and 2.065×10^{-5} K^{-1}[43] and for ferrite, 1.24×10^{-5} K^{-1}[43] and ~1.10×10^{-5} K^{-1}.[44] The results of converting the α_L into the RA fraction are presented in Figure 7.

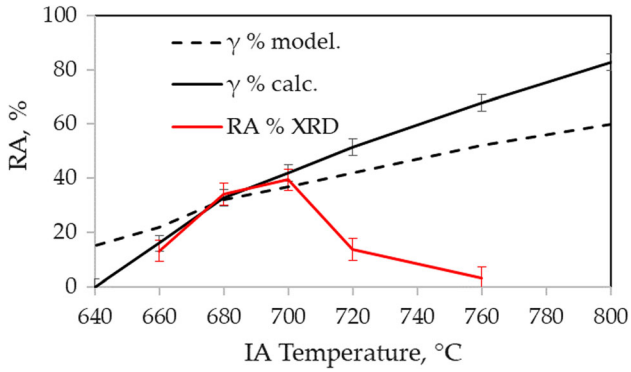

Fig. 7—Results of high-temperature austenite and RA fraction obtained by modeling, calculation of linear expansion coefficient, and XRD method; γ pct model—results of calculations using JMatPro; γ pct calc.—results obtained using Eq. [2]; and RA pct XRD—results obtained using XRD method.

The XRD results (Figure 7) indicate that RA appears only in samples annealed in a temperature range from 660 °C to 760 °C. Sample IA640 does not show any RA in the microstructure, which is consistent with dilatometric data. The RA fraction after quenching increases with the increase of the IA temperature and reaches maximum values in the case of samples IA680 (35 pct) and IA700 (39.5 pct). After exceeding 700 °C, the RA amount decreases, as a result of the martensitic transformation confirmed by dilatometry (up to 0 pct in the case of sample IA800). The experimental results (XRD) and those calculated by means of thermal expansion coefficient are in good agreement in the range 640 °C to 700 °C, where martensitic transformation is not recorded in dilatometry. The obtained results indicate the correctness of the proposed method. An additional advantage is that the calculation of the amount of RA concerns a given moment in the process (immediately before quenching), while the *in-situ* XRD test runs for a given time,[21,22] depending on the parameters used, and the obtained value is, therefore, the average value from a given measurement time.

The model results calculated using JMatPro differ from the experimental ones. However, they concern the state of equilibrium, whereas the experiments are not in equilibrium conditions. This is visible in Figure 8(a), which shows a comparison of the model and calculated (XRD) and measured (EDS) concentrations of C and Mn in RA. It can be seen that 1 hour of IA is far too short a time to reach equilibrium conditions. The decrease of C and Mn during IA with the increase of the temperature is in agreement with literature[13] and theoretical calculations; however, the particular values are not. The Mn concentration changes in the range from 6.2 pct at 660 °C to 5.1 at 760 °C, while the equilibrium values are 10 and 6.8 pct, respectively. This difference could be explained by sluggish diffusion of manganese.[27] In the case of carbon diffusion, the trend is opposite. The XRD measurements indicate higher values (from 0.95 to 0.42 pct) than the theoretically calculated ones (from 0.56 to 0.33 pct). In this case, the higher values could be the result of three factors: (1)

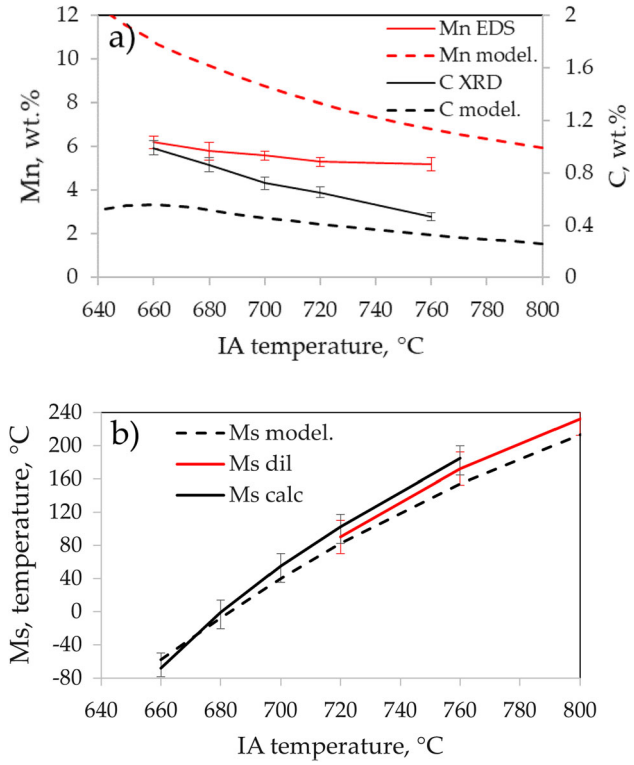

Fig. 8—Changes of (*a*) chemical element concentration in RA and (*b*) M_s temperature with increasing IA temperature; model—results of calculations using JMatPro; M_s dil. —dilatometric results; and M_s calc—results obtained using Eq. [4].

with time, the fraction of RA continuously increases up to the equilibrium condition, which causes a further reduction of the average C concentration in this phase;[45] (2) the tendency of manganese to lower the carbon concentration in RA, as shown by Sugimoto *et al.*[46] and Tanino *et al.*[47]; and (3) possible carbide precipitation after a long annealing time. It can be seen that with an increase in IA temperature, the equilibrium and nonequilibrium values of C and Mn concentration approach each other, related to the easier diffusion at higher temperatures.[13] The experimental M_s temperatures determined by dilatometry are presented in Figure 8(b). The measured Mn and C concentrations in RA were used (Eq. [4]) to calculate the theoretical values of M_s. Results of both methods are in line, although it should be noted that the commonly used equations do not take the grain size effect into consideration.[17] Furthermore, the model values of M_s fit the relation despite the differences in chemical element concentration. Despite the lower enrichment in Mn, the increased C concentration enables maintenance of the stability at a certain level. The M_s value results indicate that despite the largest fraction of RA (39.5 pct) in the IA700 sample, its thermodynamic stability is at a critical level ($M_s \sim 20$ °C), whereas the IA680 sample has an attractive combination of parameters: RA ~ 35 pct, C ~ 0.86 wt pct, Mn ~ 5.85 wt pct, and $M_s < 0$ °C.

The results of the hardness tests are presented in Figure 9. Hardness decreases from 346 to 318 HV1with the increase of the IA temperature from 640 °C to 700

°C, related to tempering of the martensite (M_T) and an increasing fraction of newly formed austenite. The hardness of the microstructures obtained after IA and quenching from temperatures above 700 °C increased significantly, reaching 489 HV1, in sample IA800. This increase is associated with the formation of large fractions of fresh martensite (M_F) during cooling.

B. *Microstructural Characterization*

The SEM images presented in Figure 10 show the evolution of microstructure at different annealing temperatures. The microstructure of the sample annealed at 640 °C (Figure 10(a)) is composed of tempered martensite with clearly visible intralath and interpolate precipitates, as presented by Mueller *et al.*[48] and Burja *et al.*[49] Large M_T plates are visible in the vicinity of the fine ones. In the case of sample IH660 (Figure 10(b)), the precipitates are still visible but only inside thick plates of M_T, which results from the diffusion distance into the austenitic areas. The RA grains start to appear (they can be distinguished from the martensite as RA shows a "smoother appearance" due to the fact that they are less prone to nital etching)[50] along the boundaries of the thick plates of tempered martensite, as reported by Varanasi *et al.*[7] and Mueller *et al.*[48] With a temperature increase to 680 °C (Figure 10(c)), the precipitates dissolve and the microstructure is composed of bright lathlike austenite and dark ferrite. A similar structure is observed in the sample IA700 (Figure 10(d)). However, with a further increase of the temperature (Figures 10(e) and (f)), the fraction of the RA is reduced in favor of fresh martensite (as recorded on the dilatometric results). All obtained micrographs show a fine-grained lathlike morphology, as a result of the ART process.[51] The austenite nucleation on martensite laths is based on two mechanisms: (1) nucleation of austenite on the high-angle boundaries and triple joints of prior (before quenching) austenite and (2) nucleation of this phase along the tempered martensite plates (nucleation of austenite along cementite precipitates).[52] The latter leads to the formation of elongated, lathlike grains of austenite (and, thus, ferrite) in line with the morphology of earlier martensitic structure. It is clear that the fraction of ferrite (tempered martensite) decreases with

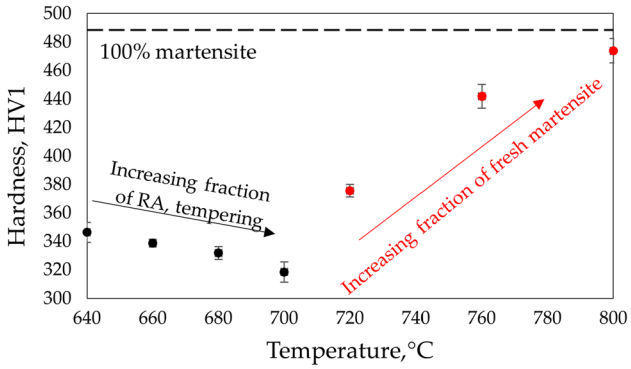

Fig. 9—Hardness results for samples annealed at different temperatures.

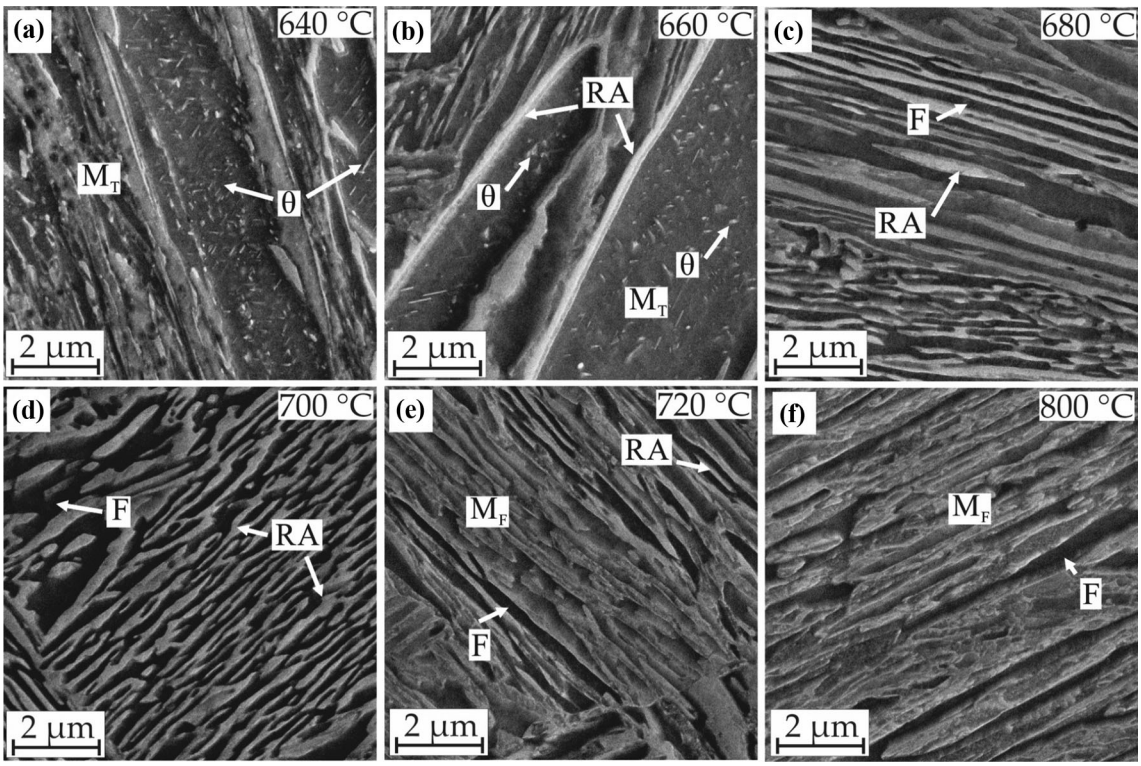

Fig. 10—SEM images of samples intercritically annealed at different temperatures: (*a*) 640 °C, (*b*) 660 °C, (*c*) 680 °C, (*d*) 700 °C, (*e*) 720 °C, and (*f*) 800 °C; RA—retained austenite; M_F—fresh martensite; M_T—tempered martensite; F—ferrite; and θ—carbides.

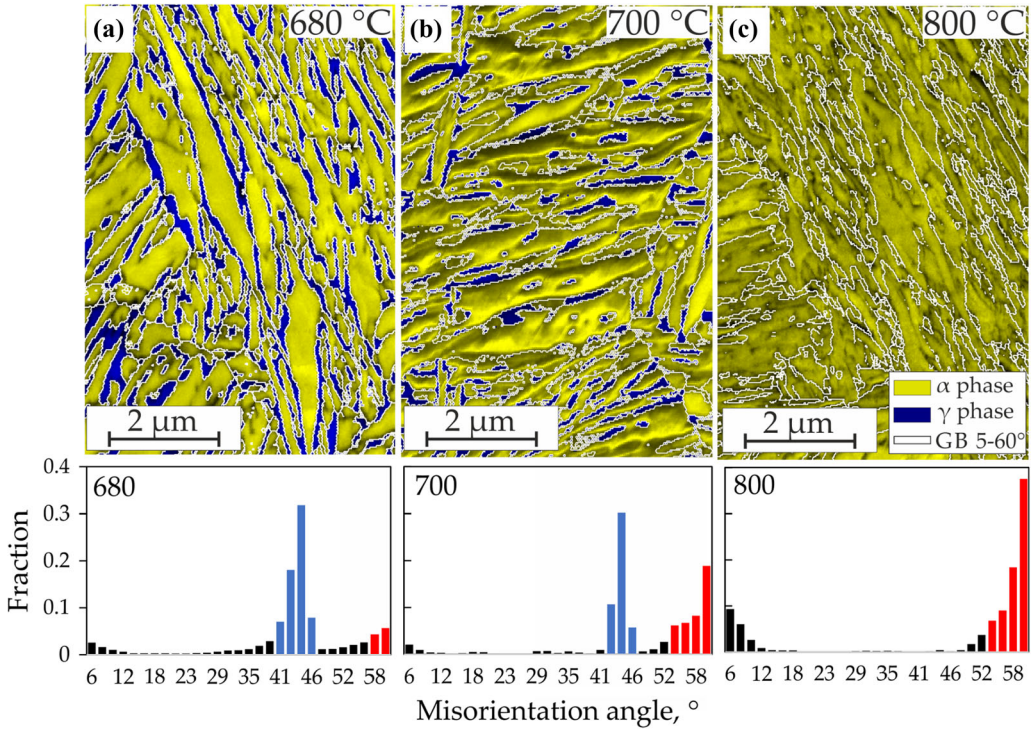

Fig. 11—IQ + phase + grain boundary maps and corresponding GB misorientation redistribution for samples (*a*) IH680, (*b*) IH700, and (*c*) IH800.

increasing temperature and is refined by increasing the fraction of formed austenite, which is consistent with the results provided by other techniques (Figures 2, 4, and 6). At lower temperatures, such as intrabath 640 °C and 660 °C (Figures 10(a) and (b)), large grains of tempered martensite are visible. After exceeding 680 °C (Figures 10(c) through (f)),which is associated with the formation of a much larger fraction of austenite, the ferritic grains are refined and reduced, leading to more homogenized microstructure.

Figure 11 shows image quality (IQ) + phase maps with the corresponding misorientation of the grain boundary distribution for variants IA680, IA700, and IA 800. It can be seen that some parts of austenite grains of samples IA6800 and IA700 transformed partially into martensite (darker regions of α phase limited by grain boundary)[53,54] despite the full stabilization indicated by XRD and dilatometry. It should be noted that all RA fraction results from the EBSD analysis are usually underestimated due to the superficial nature of the test, which is very much influenced by the sample preparation.[5] Martensitic transformation during grinding/polishing may have some impact on the results. However, it may be used for indirect and simplified determination of austenite stability: bot samples (IA 680 and IA700) were prepared under identical conditions, and the RA fraction results measured for three areas are 29.2 ± 4 (35 pct from XRD) and 19.2 ± 6 (39.5 from XRD) at 680 °C and 700 °C, respectively. Based on this relation, it is clear that in sample IA700, the amount of austenite should be higher, but its mechanical stability is significantly reduced compared to the IA680 sample. This is confirmed by M_s temperature calculations (Figure 8(b)), which show that the M_s for the IA700 sample is ~20 °C, whereas it remains below 0 °C for the IA680 sample. The RA stability in the IA700 sample reaches the critical value, which results in a high fraction of this phase measured by the XRD method. However, the mechanically affected surface measurement shows a significant part of the low-stable austenite has been transformed. The IA800 sample does not exhibit any RA in its microstructure, which is in agreement with other methods used. The formation of austenite is related to the creation of specific grain boundary angles, which are ~45 deg.[55] It can be seen that this type of boundary is occurs frequently for sample IA680 (> 80 pct) (Figure 11(a)). For sample IA700 (Figure 11(b)), its frequency decreases due to the partial martensitic transformation during sample preparation. In sample IA800 (Figure 11(c)), there is a lack of this type of boundary caused by 100 pct transformation of high-temperature austenite. The diagrams also show intensification of grain boundaries at angles > 55 deg, which are characteristic for martensite and bainite.[56,57] They appear in all samples but more clearly in the case of sample IA700, where some fraction of martensite was formed, and especially in sample IA800, composed mainly of fresh martensite.

IV. CONCLUSIONS

This work concerned the effect of temperature on the IA process in 0.17C–5Mn–1.5Al–0.2Si–0.2Mo–0.03Nb steel. The experimental research was preceded by a computational simulation of γ phase stability and changes of its chemical composition in the equilibrium state. The experimental heat treatment was carried out using the dilatometric method allowing for a thorough analysis of the process and subsequent calculation of the phase equilibrium at different annealing temperatures. The XRD and EBSD methods were used for quantitative and qualitative evaluation of the produced microstructures. The research led to the following conclusions.

1. The kinetics of austenite formation during annealing increase significantly with treatment. The completion of austenitic transformation is possible only at temperatures of 720 °C and higher within 1 hour. The half time of recorded transformation is reduced from ~12 to < 1 minutes with the temperature increase from 660 °C to 800 °C.
2. The increase of IA temperature generates a higher γ/α ratio during annealing. The maximum fraction of austenite possible to stabilize is about 39 pct, in the case of 1-hour process duration at 700 °C and bulk chemical composition (0.17C and 5Mn).
3. One hour of IA is insufficient to obtain phase and chemical equilibrium conditions, which is a reason for the observed differences between the experimental and model results.
4. The maximum fractions of RA measured by XRD were produced in the samples annealed at 680 °C (35 pct) and 700 °C (39 pct), for which $M_s \sim -5$ °C and 20 °C, respectively.
5. A newly proposed method to calculate the high-temperature phase fraction based on dilatometric results and the thermal expansion coefficient is in good agreement with experimental results.
6. The overall stability of RA deteriorates with an increase in the process temperature and, thus, a fraction of this phase. Fresh martensite forms during cooling in samples treated at temperatures higher than 700 °C, which influences the fraction of RA and material hardness.
7. Austenite nucleation in the martensite matrix during heating and subsequent annealing ensures the acquisition of fine, lathlike microstructures.

FUNDING

This research was funded by a rector grant in the area of scientific research and development works, Silesian University of Technology (Grant No. 10/010/RGJ21/1025).

CONFLICT OF INTEREST

On behalf of all of the authors, the corresponding author states that there is no conflict of interest.

REFERENCES

1. S. Ayenampudi, C. Celada-Casero, J. Sietsma, and M.J. Santofimia: *Materialia*, 2019, vol. 8, p. 100492.
2. A. Skowronek, M. Morawiec, V. Ruiz-Jimenez, C. Garcia-Mateo, and A. Grajcar: *Arch. Civ. Mech. Eng.*, 2020, vol. 20, p. 136.
3. A. Grajcar, D. Woźniak, and A. Kozłowska: *Arch. Metall. Mater.*, 2016, vol. 61, pp. 811–20.
4. Y.-G. Yang, Z.-L. Mi, M. Xu, Q. Xiu, J. Li, and H.-T. Jiang: *Mater. Sci. Eng. A*, 2018, vol. 725, pp. 389–97.
5. J. Han, S.-J. Lee, J.-G. Jung, and Y.-K. Lee: *Acta Mater.*, 2014, vol. 78, pp. 369–77.
6. Q. Lai, M. Gouné, A. Perlade, T. Pardoen, P. Jacques, O. Bouaziz, and Y. Bréchet: *Metall. Mater. Trans. A*, 2016, vol. 47A, pp. 3375–86.
7. R.S. Varanasi, M. Lipińska-Chwałek, J. Mayer, B. Gault, and D. Ponge: *Scripta Mater.*, 2022, vol. 206, p. 114228.
8. Z. Gronostajski, A. Niechajowicz, and S. Polak: *Arch. Civ. Mech. Eng.*, 2010, vol. 55, pp. 221–30.
9. K. Radwanski, R. Kuziak, and R. Rozmus: *Arch. Civ. Mech. Eng.*, 2019, vol. 19, pp. 453–68.
10. K. Kowalczyk, M. Jabłońska, S. Rusz, and G. Junak: *Arch. Metall. Mater.*, 2018, pp. 1957–61.
11. Y. Chang, C.Y. Wang, K.M. Zhao, H. Dong, and J.W. Yan: *Mater. Des.*, 2016, vol. 94, pp. 424–32.
12. A. Skowronek and A. Grajcar: *Appl. Sci.*, 2021, vol. 11, p. 9512.
13. Y.-K. Lee and J. Han: *Mater. Sci. Technol.*, 2015, vol. 31, pp. 843–56.
14. Y. Ma, W. Song, S. Zhou, A. Schwedt, and W. Bleck: *Metals*, 2018, vol. 8, p. 357.
15. A. Arlazarov, M. Goune, and A. Hazotte: *Characterization of Microstructure Formation and Mechanical Behavior of an Advanced Medium Mn Steel*, Pittsburgh, PA, 2012, pp. 1124–31.
16. F.G. Caballero, C. GarcíA-Mateo, J. Chao, M.J. Santofimia, C. Capdevila, and C.G. de Andrés: *ISIJ Int.*, 2008, vol. 48, pp. 1256–62.
17. Y.F. Shen, L.N. Qiu, X. Sun, L. Zuo, P.K. Liaw, and D. Raabe: *Mater. Sci. Eng. A*, 2015, vol. 636, pp. 551–64.
18. D. De Knijf, R. Petrov, C. Föjer, and L.A.I. Kestens: *Mater. Sci. Eng. A*, 2014, vol. 615, pp. 107–15.
19. R. Kuziak, R. Kawalla, and S. Waengler: *Arch. Civ. Mech. Eng.*, 2008, vol. 8, pp. 103–17.
20. M. Bai, D. Yang, G. Wang, J. Ryu, K. Lee, and H. Yi: *Metals*, 2020, vol. 10, p. 1432.
21. X. Hu, J.J. Mueller, X. Sun, E. De Moor, J.G. Speer, D.K. Matlock, and Y. Ren: *Front. Mater.*, 2021, vol. 8, p. 621784.
22. C. Hu, P. Liu, and Y. Liu: *Procedia Eng.*, 2011, vol. 24, pp. 404–11.
23. F.G. Caballero, C. Garcia-Mateo, and C. Garcia De Andres: *Mater. Trans.*, 2005, vol. 46, pp. 581–86.
24. P. Podany, C. Reardon, M. Koukolikova, R. Prochazka, and A. Franc: *Metals*, 2018, vol. 8, p. 263.
25. E. De Moor, D.K. Matlock, J.G. Speer, and M.J. Merwin: *Scripta Mater.*, 2011, vol. 64, pp. 185–88.
26. D.T. Han, Y.B. Xu, Y. Zou, Z.P. Hu, S.Q. Chen, and Y.M. Yu: *Mater. Sci. Forum.*, 2018, vol. 941, pp. 292–98.
27. L. Král, B. Million, and J. Čermák: *Defect Diffus. Forum*, 2007, vol. 263, pp. 153–58.
28. Sente Software Ltd.: *A Collection of Free Downloadable Papers on the Development and Application of JmatPro*, https://www.sentesoftware.co.uk/biblio.html. Accessed 25 March 2020.
29. ASTM A1033-04: "Standard Practice for Quantitative Measurement and Reporting of Hypoeutectoid Carbon and Low-Alloy Steel Phase Transformations," ASTM International, West Conshohocken, PA, https://www.astm.org/. Accessed 25 July 2020.
30. H.-S. Yang and H.K.D.H. Bhadeshia: *Mater. Sci. Technol.*, 2007, vol. 23, pp. 556–60.
31. J. Zhang, D.-F. Chen, C.-Q. Zhang, W.-S. Hwang, and M.-R. Han: *Mater. Res.*, 2015, vol. 30, pp. 2081–89.
32. N. van Dijk, A. Butt, L. Zhao, J. Sietsma, S. Offerman, J. Wright, and S. Zwaag: *Acta Mater.*, 2005, vol. 53, pp. 5439–47.
33. K. Radwański: *Arch. Civ. Mech. Eng.*, 2016, vol. 16, pp. 282–93.
34. S.I. Wright and M.M. Nowell: *Microsc. Microanal.*, 2006, vol. 12, pp. 72–84.
35. J. Trzaska: *Arch. Metall. Mater.*, 2015, vol. 60, pp. 181–85.

36. L. De Carvalho, M. Andrade, R. Lesley, F. Souza, and A. Padilha: *Mater. Res.*, 2013, vol. 16, pp. 740–44.
37. D. Fonseca, A. Feitosa, M. Feitosa, L. De Carvalho, R. Lesley, and A. Padilha: *Mater. Res.*, 2021, vol. 24, p. 20200470.
38. H. Xu, W. Cao, H. Dong, and J. Li: *ISIJ Int.*, 2015, vol. 55, pp. 662–69.
39. J. Hidalgo, C. Celada-Casero, and M.J. Santofimia: *Mater. Sci. Eng. A*, 2019, vol. 754, pp. 766–77.
40. A. Navarro-López, J. Sietsma, and M.J. Santofimia: *Metall. Mater. Trans. A*, 2016, vol. 47A, pp. 1028–39.
41. H. Talebi, M. Jahazi, and H. Melkonyan: *Materials*, 2018, vol. 11, p. 1441.
42. M. Onsøien, M. M'Hamdi, and A. Mo: *Weld. J.*, 2009, vol. 88, pp. 1S-6S.
43. F.G. Caballero, C. Capdevila, and C.G.D. Andrés: *ISIJ Int.*, 2001, vol. 41, pp. 1093–1102.
44. S. Kobayashi, and H. Fukunishi: *ISIJ Int.* 2020, vol. 60, pp. 2983–89.
45. A. Arlazarov, M. Goune, O. Bouaziz, A. Hazotte, and F. Kegel: *Materials Science Forum*, Trans Tech Publications, Quebec City, 2011, pp. 706–09.
46. K. Sugimoto, N. Usui, M. Kobayashi, and S. Hashimoto: *ISIJ Int.*, 1992, vol. 32, pp. 1311–18.
47. H. Tanino, M. Horita, and K.-I. Sugimoto: *Metall. Mater. Trans. A*, 2016, vol. 47A, pp. 2073–80.
48. J.J. Mueller, X. Hu, X. Sun, Y. Ren, K. Choi, E. Barker, J.G. Speer, D. Matlock, and E. De Moor: *Mater. Des.*, 2021, vol. 203, p. 109598.
49. J. Burja, B. Šuler, M. Češnjaj, and A. Nagode: *Metals*, 2021, vol. 11, p. 392.
50. H. Roumen, S. Juri, and A. Leo, eds.: in *Encyclopedia of Iron, Steel, and Their Alloys*, CRC Press, Boca Raton, 2016.
51. B. Hu and H. Luo: *Metals*, 2017, vol. 7, p. 464.
52. R. Schneider, K. Steineder, D. Krizan, and C. Sommitsch: *Mater. Sci. Technol.*, 2019, vol. 35, pp. 2045–53.
53. J. Wu, P.J. Wray, C.I. Garcia, M. Hua, and A.J. Deardo: *ISIJ Int.*, 2005, vol. 45, pp. 254–62.
54. M.J. Santofimia, R.H. Petrov, L. Zhao, and J. Sietsma: *Mater. Charact.*, 2014, vol. 92, pp. 91–95.
55. K. Verbeken, L. Barbé, and D. Raabe: *ISIJ Int.*, 2009, vol. 49, pp. 1601–09.
56. S. Zajac, V. Schwinn, and K.-H. Tacke: *Mater. Sci. Forum.*, 2005, vol. 500–501, pp. 387–94.
57. A. Kaijalainen, M. Liimatainen, V. Kesti, J. Heikkala, T. Liimatainen, and D. Porter: *Metall. Mater. Trans. A*, 2016, vol. 47A, pp. 4175–88.